Identification of an excitonic phonon sideband by photoluminescence spectroscopy of single-walled carbon-13 nanotubes

Yuhei Miyauchi and Shigeo Maruyama*
Department of Mechanical Engineering, The University of Tokyo, 7-3-1 Hongo, Bunkyo-ku, Tokyo 113-8656, Japan
(Received 3 January 2006; revised manuscript received 13 April 2006; published 14 July 2006)

We have studied photoluminescence and resonant Raman scattering of single-walled carbon nanotubes (SWNTs) consisting of carbon-13 ($SW^{13}CNTs$) synthesized from a small amount of isotopically modified ethanol. There was almost no change in the Raman spectra shape for $SW^{13}CNTs$ except for a downshift of the Raman shift frequency by the square root of the mass ratio 12/13. By comparing photoluminescence excitation spectra of $SW^{13}CNTs$ and normal SWNTs, the excitonic phonon sideband due to strong exciton-phonon interaction was clearly identified with the expected isotope shift. In addition to the direct experimental proof of the strong exciton-phonon interaction, we also found low-intensity "pure electronic" features whose origin has never been elucidated.

DOI: 10.1103/PhysRevB.74.035415 PACS number(s): 78.67.Ch, 78.30.Na, 78.55.Kz, 81.07.De

Photoluminescence (PL) of single-walled carbon nanotubes (SWNTs) has been intensively investigated for the optical characterization of SWNTs.[1–8] By plotting PL emission intensities as a function of emission and excitation photon energy, Bachilo *et al.*[2] obtained a two-dimensional map of relative emission intensities. Hereafter, we refer to such a plot of PL spectra of SWNTs as a "PL map." A peak in a PL map corresponds to the excitation transition energy of the second subband (E_{22}) and the photon emission energy of the first subband (E_{11}) of a specific SWNT, which can be used for assignment of chiral indices (n,m).[2,9] Theoretical studies and recent experiments have demonstrated that these optical transitions in SWNTs are dominated by strongly correlated electron-hole states in the form of excitons.[10–13] Since these pairs of transition energies depend on the nanotube structure, we can separately measure a photoluminescence excitation (PLE) spectrum from specific (n,m) SWNTs as a cross section of the PL map at an energy corresponding to the emission of the relevant SWNTs. As far as semiconducting SWNTs are concerned, such PL mapping is one of the most promising approaches for the determination of the structure distribution in a bulk SWNT sample, if combined with an appropriate theoretical estimation of relative PL intensities depending on the electronic structure specific to each (n,m) type.[14,15] Hence, photoluminescence spectroscopy is a powerful tool not only for investigation of electronic properties of SWNTs but also in advancing toward (n,m)-controlled synthesis of SWNTs, which has never been achieved.

In a PL map, one can generally find some peaks other than bright PL peaks already assigned to particular nanotube species, whose origin has not been clearly elucidated.[2,5,6] Recently, some PL peaks from DNA-wrapped nanotubes[16] were explained by a phonon-assisted excitonic absorption and recombination process.[17] On the other hand, theoretical prediction of the excitonic phonon sideband shape[18] was in good agreement with the PL spectrum from an individual nanotube[19] and isolated SWNTs in surfactant suspension.[20] These previous experimental observations of sideband features[16,19,20] are mainly for the excitation energy range close to the E_{11} transition energy using a tunable Ti:sapphire laser, and the observed sidebands are attributed to excitation to the exciton-phonon bound state. However, the previous interpretations were based on only a peak position and lineshape analysis. Hence, the direct experimental verification of the origin of the sideband peaks is still needed for further understanding of strong electron-phonon coupling in SWNTs. Furthermore, there has been no experimental study focused on the sideband for the excitation energy range corresponding to E_{22} transition energies, despite the importance of the energy range for the measurement of relative PL intensities of each (n,m) type. Since these sideband features may overlap with other PL peaks of various (n,m) nanotubes, it is necessary to understand the origin of all the features in a PL map in the excitation energy range corresponding to E_{22} transition for the accurate measurement of relative PL intensities.

In this report, we therefore investigate experimentally these sideband peaks using SWNTs consisting of carbon-13 isotope ($SW^{13}CNTs$). Here, we mainly focus on isotope effect on PLE spectra of (7, 5) nanotubes, which have strong PL intensity in our samples. Since the energy distance between the main absorption peak and corresponding sideband mainly depends on the related optical phonon energy,[18] reduction of the energy distance is expected for $SW^{13}CNTs$ due to smaller phonon energy.

We observed isotope shift of the sideband at 0.2 to 0.3 eV above the main absorption peak corresponding to E_{22} transition. The phonon energies of SWNTs and $SW^{13}CNTs$ were confirmed to differ by a factor of square root of mass ratio using Raman spectroscopy. We also observed a similar isotope shift of sideband peaks corresponding to E_{11} transition of (7, 5) SWNTs and E_{22} transition of (6, 5) SWNTs.

In addition, we also found a low-intensity peak around ~0.57 eV above (~0.1 eV below) the E_{11} (E_{22}) transition energy with no distinct isotopic shift, although ~20 meV shift is expected if the peak was a E_{11} exciton+multiple phonon sideband as reported by Htoon *et al.*[19] This result indicates the presence of unassigned electronic transitions other than the main absorbtion peak and phonon sideband in PLE spectra of SWNTs.

We synthesized $SW^{13}CNTs$ from 0.5 grams of isotopically modified ethanol (1,2-$^{13}C_2$, 99%, Cambridge Isotope

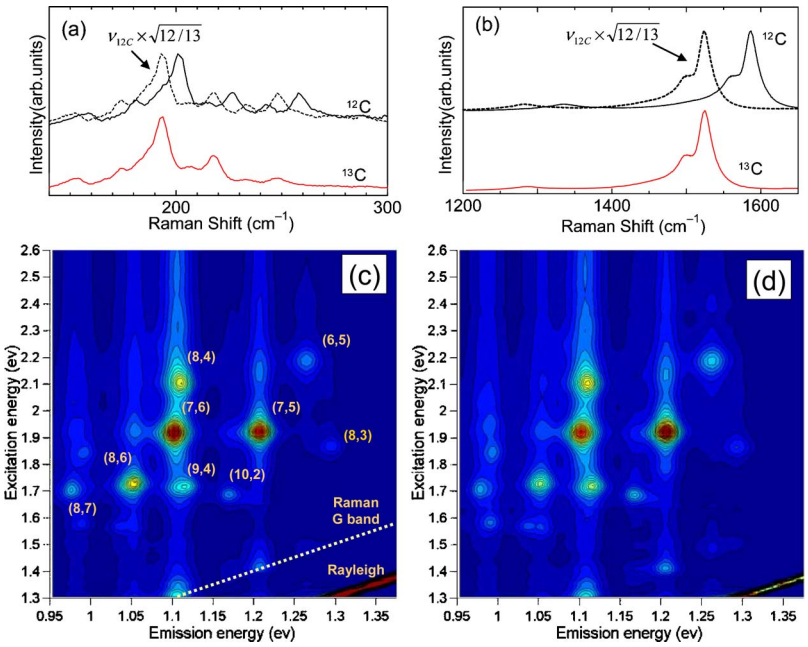

FIG. 1. (Color online) Raman spectra measured with a 488 nm (2.54 eV) excitation laser and PL maps of normal SWNTs and SW^{13}CNTs. (a) RBM, (b) *G* band. Dotted lines are spectra of normal SWNTs shifted by multiplying the Raman shift frequency by the mass ratio factor $\sqrt{12/13}$. PL maps of (c) normal SWNTs and (d) SW^{13}CNTS.

Laboratories, Inc.) by the alcohol catalytic chemical vapor deposition (ACCVD) method[21,22] optimized for the efficient production of SWNTs from a very small amount of ethanol, which is similar to the technique used for the SWNT synthesis from fullerene.[23] Further details of the synthesis of SW^{13}CNTs are presented in Ref. 24.

In order to measure PL spectra from individual SWNTs in a surfactant suspension,[1] the "as-grown" material was dispersed in D_2O with 0.5 wt% sodium dodecylbenzene sulfonate (NaDDBS) (Ref. 5) by heavy sonication with an ultrasonic processor (Hielscher GmbH, UP-400S with H3/Micro Tip 3) for 1 h at a power flux level of 460 W/cm^2. These suspensions were then centrifuged (Hitachi Koki himac CS120GX with S100AT6 angle rotor) for 1 h at 386 000 g and the supernatants, rich in isolated SWNTs, were used in the PL measurements.

Near infrared emission from the sample was recorded while the excitation wavelength was scanned from VIS to NIR range. The measured spectral data were corrected for wavelength-dependent variations in the excitation intensity and detection sensitivity. The excitation and emission spectral slit widths were both 10 nm (15–50 meV for excitation and 7–15 meV for emission in the measuring range of PL map shown in Fig. 1), and scan steps were 5 nm on both axes. In addition to PL maps over a wide emission energy range, PLE spectra of (7, 5) and (6, 5) SWNTs were recorded at the emission energy of corresponding E_{22} peaks with narrower scan steps of 2 nm. For (7, 5) SWNTs, we used narrower excitation spectral slit width of 5 nm (7–28 meV in the excitation energy range of 1.3–2.6 eV) to obtain higher resolution spectra, and the PLE spectra were accumulated for 10-20 scans to improve the signal-to-noise (S/N) ratio. The PL spectra were measured with a Horiba Spex Fluorolog-3-11 spectrofluorometer with a liquid-nitrogen-cooled InGaAs near IR detector. The Raman spectra were measured using a Chromex 501is spectrometer, an Andor Technology DV401-FI CCD system, and a Seki Technotron Corp. STR250 optical system.

Figures 1(a) and 1(b) compare Raman spectra for SW^{13}CNTs and normal SWNTs excited with a 2.54 eV (488 nm) laser. There was almost no intrinsic change in Raman spectra shape for SW^{13}CNTs, but the Raman shift frequency was $\sqrt{12/13}$ times smaller, confirming phonon energies in SW^{13}CNTs are $\sqrt{12/13}$ times smaller than in normal SWNTs because of the heavier carbon atoms. The spread in the *G*-band peak at 1590 cm^{-1} (value for SW^{12}CNTs) and the smaller *D*-band signal at 1350 cm^{-1} (value for SW^{12}CNTs) for both SW^{13}CNTs and normal SW^{12}CNTs suggest that high-quality nanotubes were synthesized. The strong radial breathing mode (RBM) peaks at around 150–300 cm^{-1} were also observed for each sample.

Figures 1(c) and 1(d) show PL maps of normal SWNTs and SW^{13}CNTs. Major peaks corresponding to the main E_{22} absorption followed by the E_{11} emission are marked with (n,m) indices assigned by Bachilo *et al.*,[2] and are listed in Table I. It can be confirmed that the relative PL intensities between different (n,m) SW^{13}CNTs are similar to those of normal SWNTs. Detailed peak positions of major PL peaks of the two samples are in good agreement, indicating that the change of the atomic mass does not greatly affect the E_{11} and E_{22} transition energy and the nanotube environment are virtually unchanged. Strictly speaking, there is a possibility of a minor isotopic energy shift even for the E_{11} and E_{22} transition energies because of the different exciton-phonon coupling due to the different atomic mass. Taking into account polaronic binding as predicted by Perebeinos *et al.*,[18] a different amount of phonon-related band-gap renormalization for SW^{13}CNTs and normal SWNTs can be expected. However, it is difficult to discuss the change of the exciton-phonon binding energy based on the apparently very small difference of the observed transition energies for the main peaks of (7, 5) and (6, 5) SWNTs in this study.

Figure 2 compares PL maps and PLE spectra of normal SWNTs and SW^{13}CNTs for (7, 5) tubes. PLE spectra in Fig. 2(c) correspond to vertical cuts of the PL maps at the emission energy indicated by solid lines in Figs. 2(a) and 2(b).

TABLE I. PL maxima of normal SWNTs and SW^{13}CNTs dispersed in D_2O/NaDDBS and their assignment.

(n,m) and Label	Emission (eV)[a]		Excitation (eV)[a]		Phonon Assisted
	^{12}C	^{13}C	^{12}C	^{13}C	
(7,5) *A*	1.208	1.206	1.416	1.409	*x*
(7,5) *B*	1.207	1.206	1.790	1.788	—
(7,5) E_{22}	1.208	1.206	1.924	1.923	—
(7,5) *C*	1.208	1.206	2.146	2.139	*x*
(6,5) *B′*	1.265	1.262	1.935	1.937	—
(6,5) E_{22}	1.265	1.263	2.188	2.189	—
(6,5) *C′*	1.265	1.262	2.404	2.396	*x*
(8,3) E_{22}	1.295	1.293	1.867	1.865	—
(10,2) E_{22}	1.170	1.167	1.687	1.686	—
(9,4) E_{22}	1.116	1.116	1.717	1.720	—
(8,4) E_{22}	1.111	1.111	2.105	2.103	—
(7,6) E_{22}	1.103	1.102	1.919	1.920	—
(8,6) E_{22}	1.054	1.054	1.731	1.730	—

[a]E_{22} excitation energies for (7,5) and (6,5) were determined by Lorentzian fittings. For all other peaks, PL emission and excitation energies were determined to an accuracy of ±0.2% using bicubic interpolations from the PL map shown in Fig. 1.

Each PLE spectrum is normalized by the E_{22} peak intensity for comparison. It can be seen that the PLE spectra exhibit a sideband 0.2–0.3 eV above the E_{22} main absorption peak (peak *C*). In addition to peak *C*, we observed a sideband peak 0.2–0.3 eV above the E_{11} main peak (peak *A*) and low-intensity structure around ~0.57 eV above (~0.1 eV below) the E_{11} (E_{22}) transition energy (peak *B*). Since the emission energies of these peaks were almost identical with that of the E_{22} absorption peak as in Table I, these peaks are also attributed to photon emission from (7, 5) nanotubes. It can be seen from Fig. 2(c) that the energy difference of peak *C* from the main E_{22} peak is reduced considerably for the PLE spectrum of SW^{13}CNTs.

To further investigate details of the difference of PLE spectra, in Fig. 3, we show the dependence of the PLE spectra of (7, 5) nanotubes scanned through the PL emission lines with the different central energy of the detection slit. Figure 3(a) shows the PL emission spectra at the E_{22} peak maxima in the PLE spectra. PL emission full width at half maximum (FWHM) linewidths are 26 meV for both samples, indicating

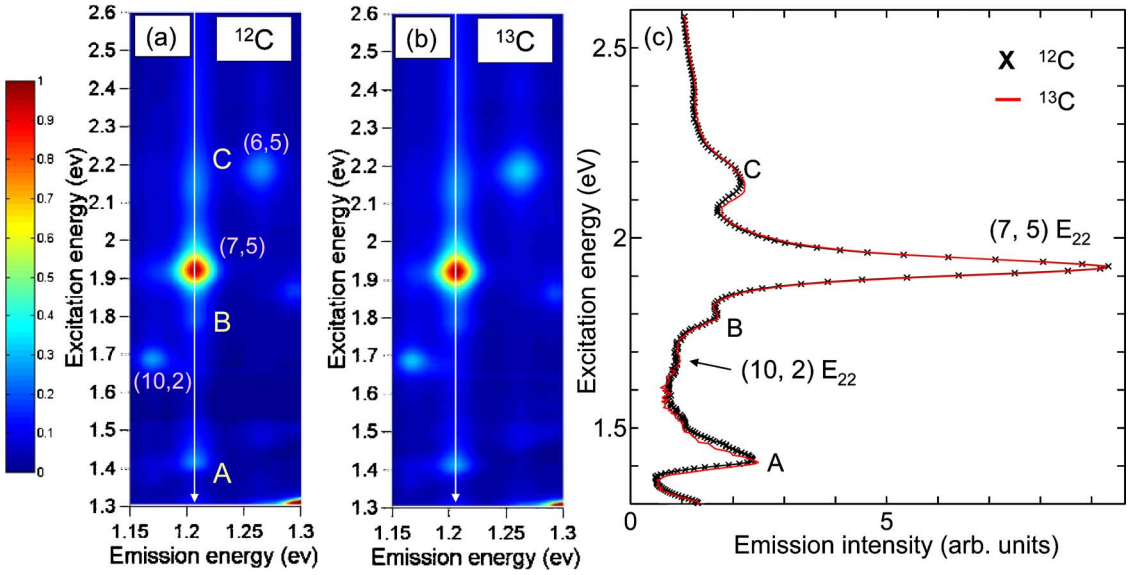

FIG. 2. (Color online) PL maps of (a) normal SWNTs and (b) SW^{13}CNTs dispersed in surfactant suspension. (c) Comparison of PLE spectra of SW^{13}CNTs and normal SWNTs at the E_{11} emission energy of (7, 5) nanotubes. Each PLE spectrum was measured along the PL emission energy of 1.208 eV.

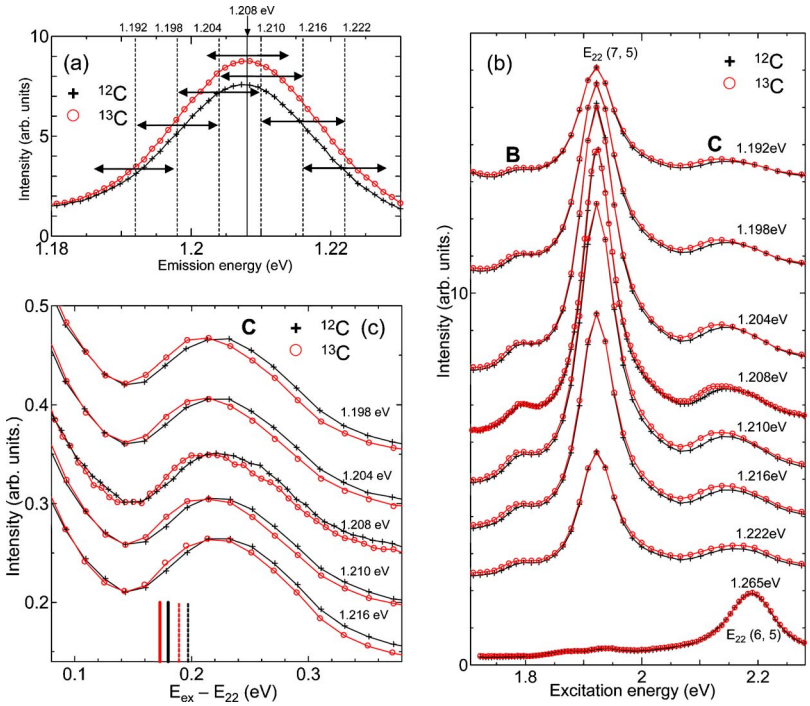

FIG. 3. (Color online) Comparison of (a) PL emission spectra at the E_{22} transition energy of (7, 5) nanotubes (1.923 eV), (b) the PLE spectra of (7, 5) nanotubes around E_{22} transition energy corresponding to the different emission energies, and (c) magnifications of the PLE spectra around peak *C* for different PL emission energies plotted as a function of energy distance from the E_{22} peak maxima. Each spectrum intensity is normalized by E_{22} intensity and the peak-top intensities are leveled for comparison in (c). Vertical dashed lines and horizontal two-headed arrows in (a) indicate the central energies of the detection slit and PL emission slit width. The red circle and black cross correspond to SW^{13}CNTs and normal SWNTs, respectively. Solid (dotted) bars in (c) represent the phonon energies of the LO phonons near the *K* (Γ) point of the graphene Brillouin zone (Refs. 18 and 25). The colors of the bars correspond to normal SWNTs (black) and SW^{13}CNTs (red).

small difference of average environment around nanotubes. Vertical dashed lines and horizontal two-headed arrows indicate the central energies of the detection slit and spectral slit width for the PLE measurements, respectively. PLE spectra at the emission energy of 1.208 eV (indicated by a solid line) were recorded with an excitation slit width of 5 nm (12–22 meV in the excitation energy range of 1.7–2.3 eV). For other emission energies, we used a 10 nm slit width (23–43 meV in the excitation energy range of 1.7–2.3 eV).

Figure 3(b) compares the PLE spectra corresponding to the different emission energies. Each spectrum is normalized by the E_{22} peak maximum of the respective PLE lines of SW^{13}CNTs for comparison. Relative intensities of E_{22} peaks correspond to the PL emission profile shown in Fig. 3(a). Variations in E_{22} energy are quite small, as in Table I, and the PLE profiles around E_{22} peaks of both samples are in good agreement throughout the PL emission energies from 1.192–1.222 eV. In the case of 5 nm excitation slit width (~15 meV around the E_{22} energy, PLE spectra at 1.208 eV), the PLE linewidths are 71 meV and 73 meV for normal SWNTs and SW^{13}CNTs, respectively. For the PLE spectra scanned with a 10 nm slit width, the linewidths are 82–85 meV and 85–88 meV for normal SWNTs and SW^{13}CNTs, respectively. This slight broadening of E_{22} peak for SW^{13}CNTs may be related to the change of exciton-phonon coupling for SW^{13}CNTs, although it is difficult to discuss the small difference of linewidth in our measurement using wide band light source.

In contrast to the E_{22} peaks, shapes and positions of peak *C* for SW^{13}CNTs are considerably different from those for normal SWNTs. When normalized by E_{22} peaks as shown in Fig. 3(b), PL intensities of peak *C* for SW^{13}CNTs appear to be slightly larger and peak positions are down-shifted except for the case of 1.222 eV emission energy. In this case, the peak shape is considerably different from other PLE spectra. Since the emission energy of 1.222 eV is close to that of (6, 5) nanotubes [1.265 eV, PLE spectra are shown at the lowest part in Fig. 3(b)], the difference is attributed to overlap of the PL emission from (6, 5) nanotubes.

Figure 3(c) shows the magnifications of the PLE spectra around peak *C* for different PL emission energies plotted as a function of energy distance from the E_{22} peak maxima. Each spectrum-intensity is normalized by E_{22} intensity and the peak-top intensities are leveled to compare the peak positions. The peak shapes corresponding to each emission energy are in good agreement with each other, while that of 1.216 eV is slightly different due to overlap of PL emission of (6, 5) nanotubes as in the case of 1.222 eV. The energy distance between peak *C* and E_{22} energy is reduced by approximately 6–10 meV for each spectra of SW^{13}CNTs through the emission energy from 1.198 to 1.210 eV. Since the energy of a peak onset of a phonon sideband is expected to strongly depend on the energies of corresponding phonons,[18] we estimated the approximate value noted above by comparing the positions of peak onset of the normalized PLE peaks.

If the peak *C* is a excitonic phonon sideband, the amount of the isotope shift is expected to be consistent with the value estimated from the difference of phonon energies. According to theoretical prediction by Perebeinos *et al.*,[18] the longitudinal optical (LO) phonons near the Γ and *K* point of the graphene Brillouin zone[18,25] have stronger exciton-phonon coupling and are dominantly contribute to the sideband.

Assuming LO phonons [K_{LO}= ~0.18 eV, Γ_{LO}= ~0.197 eV (Refs. 18 and 25)] are dominant, the isotope shift of the phonon energy is estimated as about 7 meV (8 meV) for K_{LO} (Γ_{LO}) phonons considering the square root of mass ratio $\sqrt{12/13}$. Since the energy difference of 7–8 meV is in good agreement with the observed energy

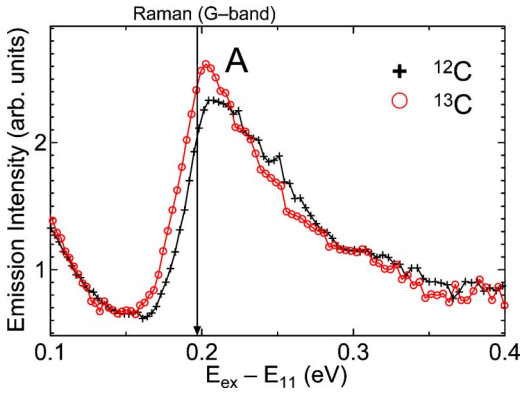

FIG. 4. (Color online) PLE spectra for peak *A* of (7, 5) nanotubes plotted as a function of energy difference from the E_{11} energy. Vertical line around ~0.2 eV indicates the energy corresponding to Raman scattering (*G* band).

shift of 6–10 meV shown in Fig. 3(c), peak *C* is identified to be an excitonic phonon sideband of the E_{22} main absorption peak due to strong exciton-phonon coupling to the LO phonons.

In Fig. 3(c), the phonon energies corresponding to the LO phonons near the *K* (Γ) point of the graphene Brillouin zone[18,25] are indicated by solid (dotted) bars. Black and red bars correspond to phonons in normal SWNTs and SW^{13}CNTs, respectively. It is clearly seen that the energy difference of peak *C* from the main PL peaks, 0.2–0.3 eV, is considerably larger than the optical phonon energy, which is no more than ~0.2 eV.[25] Here, it should be noted that the line shape and the energy difference from E_{22} are remarkably similar to the excitonic phonon sideband predicted by Perebeinos *et al.*[18] This larger energy difference of phonon sideband peaks from E_{22} peaks than optical phonon energy can be interpreted by considering phonon-assisted excitation to so-called dark (dipole-forbidden) exciton bands by K_{LO} phonons.[18] Considering the contribution of dark excitons with finite momentum *q*, the energy contribution from optical absorption required to make a finite-*q* exciton is the sum of the energy of a dark exciton and the phonon (or phonons) satisfying energy-momentum conservation. When the dark excitons that dominate the sideband have energies larger than the optically active E_{ii} exciton, the energy difference between E_{ii} and the phonon sideband peak can exceed the phonon energy.[18] The amount of contribution of dark exciton band is roughly estimated as about 40 meV for (7, 5) nanotubes by subtracting phonon energy from the observed energy difference between E_{22} peak and the sideband peak.

In contrast to peak *C*, we observed almost no distinct shift of peaks *B* as shown in Fig. 3(b), indicating that these peaks are neither Raman scattering originated nor phonon sideband peak. Taking the energy distance of peak *B* from E_{11} transition (~0.57 eV) into account, one may attribute peak *B* to multiphonon transitions as reported by Htoon *et al.*[19] Considering simultaneous excitation of one *G*-band phonon (~0.197 eV) and two *D*-band phonons (~0.335 eV),[25] one can expect a multiphonon sideband to be approximately 0.53 eV above the E_{11} transition energy. Although the energy of ~0.53 eV is smaller than the observed energy distance

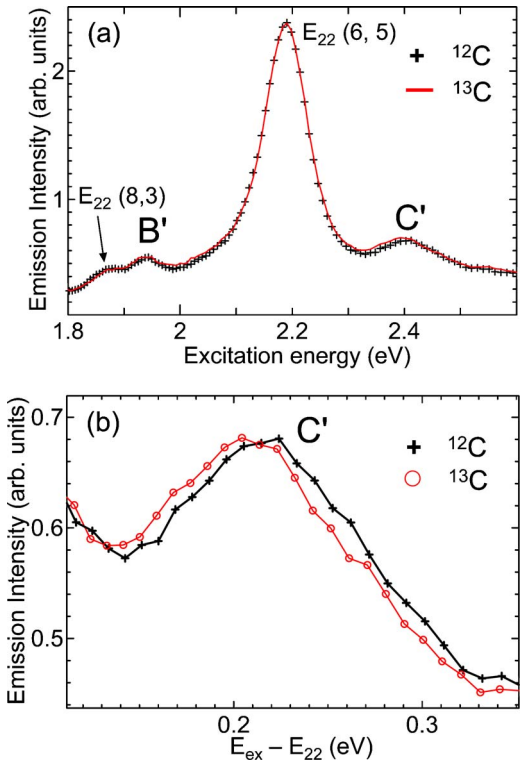

FIG. 5. (Color online) (a) PLE spectra of (6, 5) nanotubes around E_{22} transition energy, and (b) magnifications of the PLE spectra around peak *C′* for (6, 5) nanotubes plotted as a function of energy difference from the E_{22} energy. Each spectrum-intensity is normalized by E_{22} intensity and the peak-top intensities are leveled for comparison in (b).

~0.57 eV, this discrepancy is at most comparable to that of peak *C*. However, if peak *B* is a multiphonon sideband, the isotope energy shift is expected to be ~20 meV from the square root of mass ratio. We can conclude such a large energy shift is not observed even taking into consideration some ambiguity of the energy position of peak *B* due to overlaps of large E_{22} peak and PL emission from (10, 2) nanotubes. Hence, we attribute peak *B* to a "pure electronic" transition without phonon assistance.

To identify these "pure electronic" features, we have measured polarized PLE spectra of aligned nanotubes in gelatin matrix.[26] The results suggested that these features, like peak *B*, had different polarization dependence from E_{ii} peaks and phonon sideband features. We have attributed these features to optical transitions corresponding to excitation by perpendicularly polarized light to the nanotube axis.[27–29] Further details of the experiment will be presented elsewhere.[26]

In addition to the features around E_{22} transition of (7, 5) nanotubes, we also investigated isotope effect on some sideband features in a PL map. In Fig. 4, we show PLE spectra of (7, 5) nanotubes around E_{11} energy as a function of energy distance from E_{11} transition energy. Each spectrum is normalized by the E_{22} peak maxima. We observed a distinct sideband 0.2–0.3 eV above the E_{11} energy (peak *A*) as reported by Plentz *et al.*[20] They measured PLE spectra for several different SWNTs on aqueous suspension include (7, 5) nanotubes using Ti:sapphire laser in the energy range be-

tween 1.2 and 1.75 eV, and attributed the observed sideband peaks to exciton-phonon bound states by comparing the PLE line shape with that predicted by Perebeinos *et al.*[18] Here we observed the reduction of energy distance between peak *A* and E_{11} energy by approximately 5–9 meV for SW[13]CNTs, which is consistent with the result for peak *C*. With regard to peak *A*, it should be noted that Raman scattering and phonon sideband are overlapped each other. We compared the observed spectral shape of peak *A* with the corresponding spectra in Ref. 20 and confirmed that the line shape and linewidth are comparable to those measured using a tunable laser as the light source. Hence, it is reasonable to suppose that our resolution in this energy range is sufficient and the broad linewidth of peak *A* is due to the phonon-assisted excitation to the excitons with finite momentum q.

As is the case for E_{11} sideband,[19,20] E_{22} sideband is also observed for various SWNTs. Figure 5(a) compares PLE spectra of (6, 5) SW[13]CNTs and normal SWNTs normalized by the E_{22} peak maxima. In Fig. 5(a), one can find a sideband with a similar line shape to peak *C* of (7, 5) nanotubes, 0.2–0.3 eV above the E_{22} main absorption peak (peak C'). Figure 5(b) shows the magnifications of the PLE spectra around peak C' plotted as a function of energy distance from E_{22} peak maxima. Each spectrum intensity is normalized by E_{22} intensity and the peak-top intensities are leveled for comparison in Fig. 5(b). For peak C', we also observed isotope shift of 6–9 meV for SW[13]CNTs, which is in good agreement with that observed for peak *C*. Since the line shape and peak position from the E_{22} main peak are similar to those of peak *C*, we attribute peak C' to the same origin of peak *C*. In Fig. 5(a), one can also find small peak (peak B') ~0.25 eV below the E_{22} peak. Since PL emission energy around peak B' is almost identical with that around the E_{22} energy as shown in Table I, peak B' also corresponds to PL emission from (6, 5) nanotubes. Although lower signal-to-noise ratio and overlap of PL emission from (8, 3) nanotubes do not allow for a positive assignment, peak B' may be a peak that has a similar origin to peak *B* for (7, 5) nanotubes.

In conclusion, we have measured PL and Raman spectra of SW[13]CNTs and distinguished excitonic-phonon sideband peaks from those without phonon assistance by comparing PLE spectra of SW[13]CNTs and normal SWNTs. With regard to (7, 5) and (6, 5) nanotubes, three sideband peaks with energies about 0.2–0.3 eV larger than E_{ii} transition energies were identified as excitonic-phonon sidebands, while the PL peaks of (7, 5) nanotubes without the isotopic shift were attributed to a "pure electronic" excitation without phonon assistance.

The authors are grateful to E. Einarsson, J. Shiomi (The University of Tokyo), and S. Chiashi (Tokyo University of Science) for valuable discussions. The work is supported in part by the Japan Society for the Promotion of Science for Young Scientists Grant No. 16-11409 and Grants-in-Aid for Scientific Research No. 16360098 and No. 13GS0019.

*Corresponding author. Electronic address: maruyama@photon.t.u-tokyo.ac.jp

[1] M. J. O'Connell, S. M. Bachilo, C. B. Huffman, V. C. Moore, M. S. Strano, E. H. Haroz, K. L. Rialon, P. J. Boul, W. H. Noon, C. Kittrell, J. Ma, R. H. Hauge, R. B. Weisman, and R. E. Smalley, Science **297**, 593 (2002).

[2] S. M. Bachilo, M. S. Strano, C. Kittrell, R. H. Hauge, R. E. Smalley, and R. B. Weisman, Science **298**, 2361 (2002).

[3] A. Hartschuh, H. N. Pedrosa, L. Novotny, and T. D. Krauss, Science **301**, 1354 (2003).

[4] S. Lebedkin, F. Hennrich, T. Skipa, and M. M. Kappes, J. Phys. Chem. B **107**, 1949 (2003).

[5] S. M. Bachilo, L. Balzano, J. E. Herrera, F. Pompeo, D. E. Resasco, and R. B. Weisman, J. Am. Chem. Soc. **125**, 11186 (2003).

[6] Y. Miyauchi, S. Chiashi, Y. Murakami, Y. Hayashida, and S. Maruyama, Chem. Phys. Lett. **387**, 198 (2004).

[7] J. Lefebvre, J. M. Fraser, P. Finnie, and Y. Homma, Phys. Rev. B **69**, 075403 (2004).

[8] S. G. Chou, H. B. Ribeiro, E. B. Barros, A. P. Santos, D. Nezich, Ge. G. Samsonidze, C. Fantini, M. A. Pimenta, A. Jorio, F. P. Filho, M. S. Dresselhaus, G. Dresselhaus, R. Saito, M. Zheng, G. B. Onoa, E. D. Semke, A. K. Swan, M. S. Ünlü, and B. B. Goldberg, Chem. Phys. Lett. **397**, 296 (2004).

[9] R. Saito, G. Dresselhaus, and M. S. Dresselhaus, *Physical Properties of Carbon Nanotubes* (Imperial College Press, London, 1998).

[10] T. Ando, J. Phys. Soc. Jpn. **66**, 1066 (1997).

[11] C. D. Spataru, S. Ismail-Beigi, L. X. Benedict, and S. G. Louie, Phys. Rev. Lett. **92**, 077402 (2004).

[12] V. Perebeinos, J. Tersoff, and Ph. Avouris, Phys. Rev. Lett. **92**, 257402 (2004).

[13] F. Wang, G. Dukovic, L. E. Brus, and T. F. Heinz, Science **308**, 838 (2005).

[14] S. Reich, C. Thomsen, and J. Robertson, Phys. Rev. Lett. **95**, 077402 (2005).

[15] Y. Oyama, R. Saito, K. Sato, J. Jiang, Ge. G. Samsonidze, A. Grüneis, Y. Miyauchi, S. Maruyama, A. Jorio, G. Dresselhaus, and M. S. Dresselhaus, Carbon **44**, 873 (2006).

[16] S. G. Chou, F. Plentz, J. Jiang, R. Saito, D. Nezich, H. B. Ribeiro, A. Jorio, M. A. Pimenta, Ge. G. Samsonidze, A. P. Santos, M. Zheng, G. B. Onoa, E. D. Semke, G. Dresselhaus, and M. S. Dresselhaus, Phys. Rev. Lett. **94**, 127402 (2005).

[17] J. Jiang, R. Saito, A. Grüneis, S. G. Chou, Ge. G. Samsonidze, A. Jorio, G. Dresselhaus, and M. S. Dresselhaus, Phys. Rev. B **71**, 045417 (2005).

[18] V. Perebeinos, J. Tersoff, and Ph. Avouris, Phys. Rev. Lett. **94**, 027402 (2005).

[19] H. Htoon, M. J. O'Connell, S. K. Doorn, and V. I. Klimov, Phys. Rev. Lett. **94**, 127403 (2005).

[20] F. Plentz, H. B. Ribeiro, A. Jorio, M. S. Strano, and M. A. Pimenta, Phys. Rev. Lett. **95**, 247401 (2005).

[21] S. Maruyama, R. Kojima, Y. Miyauchi, S. Chiashi, and M. Kohno, Chem. Phys. Lett. **360**, 229 (2002).

[22] Y. Murakami, Y. Miyauchi, S. Chiashi, and S. Maruyama, Chem. Phys. Lett. **374**, 53 (2003).
[23] S. Maruyama, Y. Miyauchi, T. Edamura, Y. Igarashi, S. Chiashi, and Y. Murakami, Chem. Phys. Lett. **375**, 553 (2003).
[24] S. Maruyama and Y. Miyauchi, AIP Conf. Proc. **786**, 100 (2005).
[25] M. S. Dresselhaus and P. C. Eklund, Adv. Phys. **49**, 705 (2000).
[26] Y. Miyauchi and S. Maruyama (unpublished).
[27] H. Ajiki and T. Ando, Physica B **201**, 349 (1994).
[28] I. Bozovic, N. Bozovic, and M. Damnjanovic, Phys. Rev. B **62**, 6971 (2000).
[29] A. Grüneis, R. Saito, Ge. G. Samsonidze, T. Kimura, M. A. Pimenta, A. Jorio, A. G. Souza Filho, G. Dresselhaus, and M. S. Dresselhaus, Phys. Rev. B **67**, 165402 (2003).